Hindawi
Mathematical Problems in Engineering
Volume 2019, Article ID 7231962, 15 pages
https://doi.org/10.1155/2019/7231962

Research Article

Interaction Analysis of Collinear Two Cracks with Unequal Length under Uniaxial Traction

Bin Yu,[1] **Jingyi Xi**,[2] **Zhonghui Chen**,[3] **and Lingfan Zhang**[3]

[1]*Datong Coal Mine Group Co., Ltd, Datong 037003, China*
[2]*China Building Technology Group Co., Ltd, Beijing 100013, China*
[3]*College of Mechanics and Civil Engineering, China University of Mining & Technology (Beijing), Beijing 100083, China*

Correspondence should be addressed to Lingfan Zhang; zhanglf@student.cumtb.edu.cn

Received 29 January 2019; Revised 10 April 2019; Accepted 11 April 2019; Published 22 May 2019

Academic Editor: Sylwester Samborski

The interaction among different sizes of cracks in materials is one of the key factors leading to the damage of brittle materials. Based on the Kachanov method, the expressions for the stress intensity factors of two collinear cracks with unequal length were obtained and the interaction effect was analyzed. A compression test of a cement mortar specimen containing two cracks and numerical analysis using RFPA^{2D} were performed. The results indicate that the crack interaction can almost be neglected when the crack distance reaches the length of the large crack; the two respective collinear cracks in the specimen grow and do not affect each other when the crack distance reaches the large crack length. The results of compression test and numerical analysis are both in agreement with the theoretical result.

1. Introduction

Brittle materials, such as rocks, concrete, and ceramics, contain a large number of inhomogeneities, such as soft and hard inclusions, pores and microcracks. These microdefects finally lead to failure under loads. An important problem in the failure behavior of materials is the interaction effect among cracks because it is one of the key factors determining the stability and failure of material engineering. Thus, the study of the interaction effect among cracks and their propagation is of great significance.

Various methods have been proposed to analyze the interaction among cracks. The singular integral equation method [1–7] was widely used to solve the multiple crack problem, but the solutions become rather complicated if the cracks are arbitrarily spaced. Taking the displacements as unknown, the work by [8–10] weakened the singularity of the integral equations and obtained approximate solutions for the interaction among cracks. Horri and Nemat-Nasser [11] and Horri [12] used the pseudo-traction method to estimate the interaction of multiple cracks in an infinite plate; however, it cannot be used to analyze the closely spaced crack problem. Gong [13] provided an exact formulation of microcrack interaction with a finite main crack. In addition, as the boundary conditions can be more readily defined for traction-free cracks, many researchers solved the crack problems by taking the traction as unknown while using the superposition technique and the idea of self-consistency [14–21]. Kachanov [14] proposed a simple method for estimating the stress intensity factors (SIFs) for cracks in elastic solids and analyzed the interaction among multiple cracks. One of the key assumptions in the Kachanov method is that the traction in a crack is assumed to be composed of a uniform component and a nonuniform component, and the effect of the nonuniform component is ignored. This method also can be used to construct the stress and displacement fields in the solid [15]. However, the accuracy of the Kachanov method depends on the configuration, especially on the distance between the cracks [14–18, 22]. A modified Kachanov method was proposed by Li et al. [23] for the analysis of solids with multiple cracks. The result of the modified method is more accurate than the result of the Kachanov method. As an application of the classical Schwarz-Neumann alternating technique, an alternating iteration method [19] was applied

to evaluate the SIFs for multiple interacting cracks, but the convergence became poor for the closely located crack problem. Based on the Kachanov method and the alternating iteration technique, a new method [24] was proposed to address the problem of the strongly interacted multiple cracks in an infinite plate. Regarding the crack tests, many authors have performed experiments to study crack propagation and coalescence, e.g., Horri [11], Ashby [25], Bobet and Einstein [26], and Reyes [27].

Most of the above research studies were aimed at the rock failure law and crack propagation law with two collinear equal length cracks. And the indoor test and numerical simulation analysis method are the main research means, so as to obtain the qualitative analysis results. However, in real materials engineering, the cracks are generally unequal in length and the relevant quantitative research in theory is still less. Hence, the aim of this study was to analyze the interaction between two collinear cracks of unequal lengths subjected to far-field uniform stresses. Based on the Kachanov method [14], the expressions for the SIFs at the tips of the unequal cracks were obtained, and the influence of the crack length and crack distance on the interaction was analyzed.

2. Calculation: Two Collinear Cracks of Unequal Length

2.1. Two Unequal Collinear Cracks Loaded by Uniaxial Tension. Let us consider an infinite plate x-o-y containing two cracks (Figure 1). The cracks incline at angles α and are loaded by uniaxial tension p^{∞} at infinity. By the superposition principle, the problem is equivalent to the following: traction p^{∞} is applied to the crack faces, and the stresses vanish at infinity. In accordance with the concept of self-consistency, this problem can be represented as a superposition of two subproblems, each containing only one crack, with each crack loaded by unknown tractions. The unknown tractions are pseudo-tractions and can be decomposed into a uniform component and a nonuniform component (Figure 2). The key assumption is to neglect the traction on one crack due to the nonuniform load on the other crack. The coordinates of crack tips are A($-b$,0), B($-k$,0), C(k,0), and D(c,0). ξ_1 and ξ_2 are local coordinate axes.

According to the assumption, the stress shed on crack 1 by crack 2 is only due to the uniform average traction on crack 2. Therefore, the explicit expression for the traction in crack 1 is

$$p_1(\xi_1) = \begin{Bmatrix} p_{n1}(\xi_1) \\ p_{t1}(\xi_1) \end{Bmatrix} = \begin{Bmatrix} p_{n1}^{\infty} + \Delta p_{21}^{n}(\xi_1) \\ p_{t1}^{\infty} + \Delta p_{21}^{t}(\xi_1) \end{Bmatrix} = \begin{Bmatrix} -\frac{1}{2}p^{\infty}(1+\cos 2\alpha) + f_{21}^{nn}\langle p_{n2}(\xi_2)\rangle \\ -\frac{1}{2}p^{\infty}\sin 2\alpha + f_{21}^{tt}\langle p_{t2}(\xi_2)\rangle \end{Bmatrix} \quad (1)$$

where $p_{n1}(\xi_1)$ and $p_{t1}(\xi_1)$ denote the normal traction and the tangential traction on crack 1, respectively; $\Delta p_{21}^{n}(\xi_1)$ and $\Delta p_{21}^{t}(\xi_1)$ denote the normal traction and the tangential traction generated along the line ($-b$, $-k$) by crack 2, respectively;

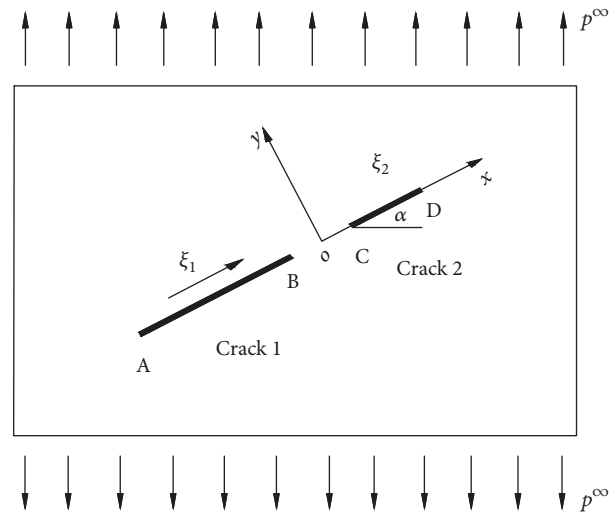

Figure 1: Two collinear cracks of unequal length in an infinite plate.

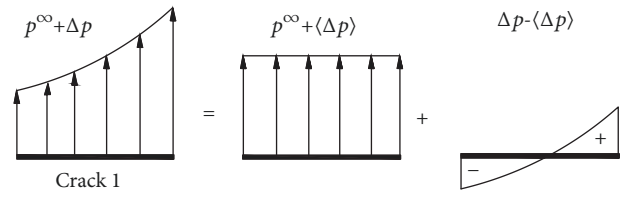

Figure 2: Decomposition of the crack traction.

$\langle p_{n2}(\xi_2)\rangle$ and $\langle p_{t2}(\xi_2)\rangle$ are the average normal traction and the average tangential traction on crack 2, respectively; f_{21}^{nn} and f_{21}^{tt} are the interaction coefficients; f_{21}^{nn} is the normal traction on crack 1 resulting from the normal uniform load of unit intensity on crack 2; f_{21}^{tt} is the shear traction on crack 1 resulting from the shear uniform load of unit intensity on crack 2. The traction on crack 2 is

$$p_2(\xi_2) = \begin{Bmatrix} p_{n2}(\xi_2) \\ p_{t2}(\xi_2) \end{Bmatrix} = \begin{Bmatrix} p_{n2}^{\infty} + \Delta p_{12}^{n}(\xi_2) \\ p_{t2}^{\infty} + \Delta p_{12}^{t}(\xi_2) \end{Bmatrix} = \begin{Bmatrix} -\frac{1}{2}p^{\infty}(1+\cos 2\alpha) + f_{12}^{nn}\langle p_{n1}(\xi_1)\rangle \\ -\frac{1}{2}p^{\infty}\sin 2\alpha + f_{12}^{tt}\langle p_{t1}(\xi_1)\rangle \end{Bmatrix} \quad (2)$$

where $\Delta p_{12}^{n}(\xi_2)$ and $\Delta p_{12}^{t}(\xi_2)$ are the normal traction and the tangential traction generated along the line (k, c) by crack 1, respectively; f_{12}^{nn} and f_{12}^{tt} are the interaction coefficients; f_{12}^{nn} is the normal traction on crack 2 resulting from the normal uniform load of unit intensity on crack 1; f_{12}^{tt} is the shear traction on crack 2 resulting from the shear uniform load of

unit intensity on crack 1. According to Appendix A, one can obtain

$$f_{21}^{nn} = f_{21}^{tt} = -\frac{\xi_1 - (c+b+2k)/2}{\sqrt{(\xi_1 - (c+b+2k)/2)^2 - ((c-k)/2)^2}} - 1 \tag{3}$$

$$f_{12}^{nn} = f_{12}^{tt} = \frac{\xi_2 + (c+b+2k)/2}{\sqrt{(\xi_2 + (c+b+2k)/2)^2 - ((b-k)/2)^2}} - 1 \tag{4}$$

Their respective average tractions are

$$\Lambda_{12}^{nn} = \frac{1}{c-k}\int_{(k-c)/2}^{(c-k)/2} f_{12}^{nn}\,d\xi_2 = \frac{\sqrt{(c+b)(c+k)} - \sqrt{2k(b+k)}}{(c-k)} - 1 = \Lambda_{12}^{tt} \tag{5}$$

$$\Lambda_{21}^{nn} = \frac{1}{b-k}\int_{(k-b)/2}^{(b-k)/2} f_{21}^{nn}\,d\xi_1 = \frac{\sqrt{(k+b)(b+c)} - \sqrt{2k(k+c)}}{(b-k)} - 1 = \Lambda_{21}^{tt} \tag{6}$$

where Λ_{ij}^{kl} (i, j=1, 2; k, l=n, t) represents the interaction coefficients due to unit intensity tractions. Taking the average of (1) and (2), one obtains

$$\begin{aligned}
\langle p_{n1}(\xi_1)\rangle &= -\frac{1}{2}p^{\infty}(1+\cos 2\alpha) + \Lambda_{21}^{nn}\langle p_{n2}(\xi_2)\rangle \\
\langle p_{n2}(\xi_2)\rangle &= -\frac{1}{2}p^{\infty}(1+\cos 2\alpha) + \Lambda_{12}^{nn}\langle p_{n1}(\xi_1)\rangle
\end{aligned} \tag{7}$$

$$\begin{aligned}
\langle p_{t1}(\xi_1)\rangle &= -\frac{1}{2}p^{\infty}\sin 2\alpha + \Lambda_{21}^{tt}\langle p_{t2}(\xi_2)\rangle \\
\langle p_{t2}(\xi_2)\rangle &= -\frac{1}{2}p^{\infty}\sin 2\alpha + \Lambda_{12}^{tt}\langle p_{t1}(\xi_1)\rangle
\end{aligned} \tag{8}$$

The terms $\langle p_{n1}(\xi_1)\rangle$, $\langle p_{n2}(\xi_2)\rangle$, $\langle p_{t1}(\xi_1)\rangle$, and $\langle p_{t2}(\xi_2)\rangle$ are readily determined in terms of Λ_{ij}. Thus, according to the general formula in Appendix B, the stress intensity factors at the tips of crack 1 and crack 2 can be obtained as

K_{I} (A)

$$= \frac{p^{\infty}(1+\cos 2\alpha)}{2\sqrt{\pi a_1}}\int_{-a_1}^{a_1}\sqrt{\frac{a_1-\xi_1}{a_1+\xi_1}}\left[1 + \frac{1+\Lambda_{12}^{nn}}{1-\Lambda_{12}^{nn}\Lambda_{21}^{nn}}\cdot\left(-\frac{\xi_1-(c+b+2k)/2}{\sqrt{(\xi_1-(c+b+2k)/2)^2-((c-k)/2)^2}} - 1\right)\right]d\xi_1 \tag{9}$$

K_{I} (B)

$$= \frac{p^{\infty}(1+\cos 2\alpha)}{2\sqrt{\pi a_1}}\int_{-a_1}^{a_1}\sqrt{\frac{a_1+\xi_1}{a_1-\xi_1}}\left[1 + \frac{1+\Lambda_{12}^{nn}}{1-\Lambda_{12}^{nn}\Lambda_{21}^{nn}}\cdot\left(-\frac{\xi_1-(c+b+2k)/2}{\sqrt{(\xi_1-(c+b+2k)/2)^2-((c-k)/2)^2}} - 1\right)\right]d\xi_1 \tag{10}$$

K_{I} (C)

$$= \frac{p^{\infty}(1+\cos 2\alpha)}{2\sqrt{\pi a_2}}\int_{-a_2}^{a_2}\sqrt{\frac{a_2-\xi_2}{a_2+\xi_2}}\left[1 + \frac{1+\Lambda_{21}^{nn}}{1-\Lambda_{12}^{nn}\Lambda_{21}^{nn}}\cdot\left(\frac{\xi_2+(c+b+2k)/2}{\sqrt{(\xi_2+(c+b+2k)/2)^2-((b-k)/2)^2}} - 1\right)\right]d\xi_2 \tag{11}$$

K_{I} (D)

$$= \frac{p^{\infty}(1+\cos 2\alpha)}{2\sqrt{\pi a_2}}\int_{-a_2}^{a_2}\sqrt{\frac{a_2+\xi_2}{a_2-\xi_2}}\left[1 + \frac{1+\Lambda_{21}^{nn}}{1-\Lambda_{12}^{nn}\Lambda_{21}^{nn}}\cdot\left(\frac{\xi_2+(c+b+2k)/2}{\sqrt{(\xi_2+(c+b+2k)/2)^2-((b-k)/2)^2}} - 1\right)\right]d\xi_2 \tag{12}$$

K_{II} (A)

$$= \frac{p^{\infty}\sin 2\alpha}{2\sqrt{\pi a_1}}\int_{-a_1}^{a_1}\sqrt{\frac{a_1-\xi_1}{a_1+\xi_1}}\left[1 + \frac{1+\Lambda_{12}^{tt}}{1-\Lambda_{12}^{tt}\Lambda_{21}^{tt}}\cdot\left(-\frac{\xi_1-(c+b+2k)/2}{\sqrt{(\xi_1-(c+b+2k)/2)^2-((c-k)/2)^2}} - 1\right)\right]d\xi_1 \tag{13}$$

K_{II} (B)

$$= \frac{p^{\infty}\sin 2\alpha}{2\sqrt{\pi a_1}}\int_{-a_1}^{a_1}\sqrt{\frac{a_1+\xi_1}{a_1-\xi_1}}\cdot\left[1 + \frac{1+\Lambda_{12}^{tt}}{1-\Lambda_{12}^{tt}\Lambda_{21}^{tt}}\cdot\left(-\frac{\xi_1-(c+b+2k)/2}{\sqrt{(\xi_1-(c+b+2k)/2)^2-((c-k)/2)^2}} - 1\right)\right]d\xi_1 \tag{14}$$

K_{II} (C)

$$= \frac{p^{\infty}\sin 2\alpha}{2\sqrt{\pi a_2}}\int_{-a_2}^{a_2}\sqrt{\frac{a_2-\xi_2}{a_2+\xi_2}}\cdot\left[1 + \frac{1+\Lambda_{21}^{tt}}{1-\Lambda_{12}^{tt}\Lambda_{21}^{tt}}\cdot\left(\frac{\xi_2+(c+b+2k)/2}{\sqrt{(\xi_2+(c+b+2k)/2)^2-((b-k)/2)^2}} - 1\right)\right]d\xi_2 \tag{15}$$

K_{II} (D)

$$= \frac{p^{\infty}\sin 2\alpha}{2\sqrt{\pi a_2}}\int_{-a_2}^{a_2}\sqrt{\frac{a_2-\xi_2}{a_2+\xi_2}}\cdot\left[1 + \frac{1+\Lambda_{21}^{tt}}{1-\Lambda_{12}^{tt}\Lambda_{21}^{tt}}\cdot\left(\frac{\xi_2+(c+b+2k)/2}{\sqrt{(\xi_2+(c+b+2k)/2)^2-((b-k)/2)^2}} - 1\right)\right]d\xi_2 \tag{16}$$

where $a_1=(b-k)/2$ and $a_2=(c-k)/2$.

2.2. Two Sliding Closed Collinear Cracks of Unequal Length. Figure 3 shows two sliding closed collinear cracks in an infinite plate. Cracks subjected to uniaxial compression may close. The normal stress on the closed cracks is neglected, and the crack tips only have K_{II}. The friction on the closed cracks has a great influence on the crack propagation. The

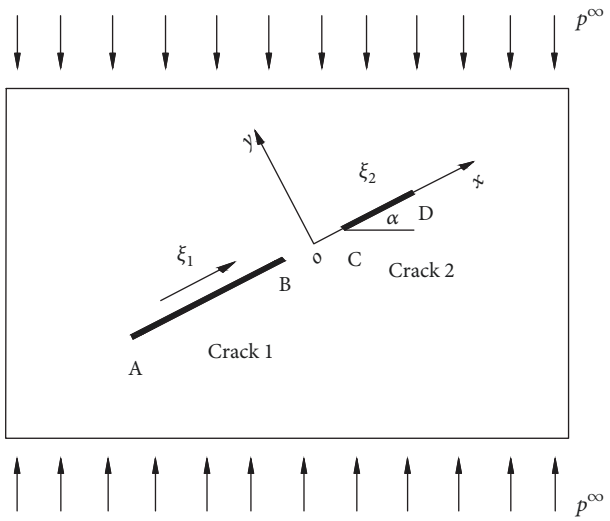

FIGURE 3: Two sliding closed collinear cracks in an infinite plate.

problem can also be represented as a superposition of two subproblems, and the superposition of the stress for two collinear closed cracks is shown in Figure 4.

Through the Coulomb-Mohr law, the actual shear stress acting on the face of the two collinear cracks in Figure 3 can be obtained as

$$\tau_{xy}^{i} = -\tau_c + \mu\sigma_y^{i} \quad (i = 1, 2) \tag{17}$$

where τ_c denotes the cohesion and μ denotes the friction coefficient. The pseudo-tractions on the cracks in the subproblems are

$$\begin{aligned} \tau_{xy}^{*i} &= \left(\tau_{xy}^{i} - \tau_{xy}^{\infty i}\right) - \Delta\tau_{xy}^{i} \\ \sigma_y^{*i} &= \left(\sigma_y^{i} - \sigma_y^{\infty i}\right) - \Delta\sigma_y^{i} \\ &\qquad (i = 1, 2) \end{aligned} \tag{18}$$

For closed cracks, $\sigma_y^{*i} = 0$; thus, the shear stress on the cracks can be obtained

$$\tau_{xy}^{*i} = -\tau_c + \mu\sigma_y^{\infty i} - \tau_{xy}^{\infty i} + \mu\Delta\sigma_y^{i} - \Delta\tau_{xy}^{i} \quad (i = 1, 2) \tag{19}$$

where $\Delta\sigma_y^{i}$ and $\Delta\tau_{xy}^{i}$ are the tractions generated by another crack, and the tractions can be obtained using the Kachanov method as follows:

$$\Delta\sigma_y^{i} = \left\langle -\sigma_y^{*j} \right\rangle f_{ji}^{nn} + \left\langle -\tau_{xy}^{*j} \right\rangle f_{ji}^{tn} \qquad (i = 1, 2;\ j = 1, 2 \text{ and } i \neq j) \tag{20}$$

$$\Delta\tau_{xy}^{i} = \left\langle -\sigma_y^{*j} \right\rangle f_{ji}^{nt} + \left\langle -\tau_{xy}^{*j} \right\rangle f_{ji}^{tt} \qquad (i = 1, 2;\ j = 1, 2 \text{ and } i \neq j) \tag{21}$$

where $\langle -\sigma_y^{*j} \rangle$ is the uniform average normal traction on the j_{th} crack and $\langle -\tau_{xy}^{*j} \rangle$ is the uniform average shear traction on the j_{th} crack. Thus, the shear stress on crack 1 is

$$\tau_{xy}^{*1} = -\tau_c + \mu\sigma_y^{\infty 1} - \tau_{xy}^{\infty 1} + \left\langle \tau_{xy}^{*2} \right\rangle f_{21}^{tt} \tag{22}$$

The shear stress on crack 2 is

$$\tau_{xy}^{*2} = -\tau_c + \mu\sigma_y^{\infty 2} - \tau_{xy}^{\infty 2} + \left\langle \tau_{xy}^{*1} \right\rangle f_{12}^{tt} \tag{23}$$

Taking the average of (22) and (23), one obtains

$$\begin{aligned} \left\langle \tau_{xy}^{*1} \right\rangle &= -\tau_c + \mu\sigma_y^{\infty 1} - \tau_{xy}^{\infty 1} + \left\langle \tau_{xy}^{*2} \right\rangle \Lambda_{21}^{tt} \\ \left\langle \tau_{xy}^{*2} \right\rangle &= -\tau_c + \mu\sigma_y^{\infty 2} - \tau_{xy}^{\infty 2} + \left\langle \tau_{xy}^{*1} \right\rangle \Lambda_{12}^{tt} \end{aligned} \tag{24}$$

By solving (24), the uniform average stress on the two unequal cracks is as follows:

$$\left\langle \tau_{xy}^{*1} \right\rangle = \frac{\left(-\tau_c + \mu\sigma_y^{\infty 1} - \tau_{xy}^{\infty 1}\right)\left(1 + \Lambda_{21}^{tt}\right)}{1 - \Lambda_{12}^{tt}\Lambda_{21}^{tt}} \tag{25}$$

$$\left\langle \tau_{xy}^{*2} \right\rangle = \frac{\left(-\tau_c + \mu\sigma_y^{\infty 2} - \tau_{xy}^{\infty 2}\right)\left(1 + \Lambda_{12}^{tt}\right)}{1 - \Lambda_{12}^{tt}\Lambda_{21}^{tt}} \tag{26}$$

Once the uniform average tractions are found, the stress intensity factors for the two unequal sliding closed cracks can be obtained

$$\begin{aligned} &K_{\text{II}}(\text{A}) \\ &= \frac{2\tau_c - \mu p^\infty (1 + \cos 2\alpha) + p^\infty \sin 2\alpha}{2\sqrt{\pi a_1}} \int_{-a_1}^{a_1} \sqrt{\frac{a_1 - \xi_1}{a_1 + \xi_1}} \left[1 \right. \\ &\left. + \frac{1 + \Lambda_{12}^{tt}}{1 - \Lambda_{12}^{tt}\Lambda_{21}^{tt}} \cdot \left(- \frac{\xi_1 - (c + b + 2k)/2}{\sqrt{\left(\xi_1 - (c + b + 2k)/2\right)^2 - \left((c - k)/2\right)^2}} - 1 \right) \right] d\xi_1 \end{aligned} \tag{27}$$

$$\begin{aligned} &K_{\text{II}}(\text{B}) \\ &= \frac{2\tau_c - \mu p^\infty (1 + \cos 2\alpha) + p^\infty \sin 2\alpha}{2\sqrt{\pi a_1}} \int_{-a_1}^{a_1} \sqrt{\frac{a_1 + \xi_1}{a_1 - \xi_1}} \left[1 \right. \\ &\left. + \frac{1 + \Lambda_{12}^{tt}}{1 - \Lambda_{12}^{tt}\Lambda_{21}^{tt}} \cdot \left(- \frac{\xi_1 - (c + b + 2k)/2}{\sqrt{\left(\xi_1 - (c + b + 2k)/2\right)^2 - \left((c - k)/2\right)^2}} - 1 \right) \right] d\xi_1 \end{aligned} \tag{28}$$

$$\begin{aligned} &K_{\text{II}}(\text{C}) \\ &= \frac{2\tau_c - \mu p^\infty (1 + \cos 2\alpha) + p^\infty \sin 2\alpha}{2\sqrt{\pi a_2}} \int_{-a_2}^{a_2} \sqrt{\frac{a_2 - \xi_2}{a_2 + \xi_2}} \left[1 \right. \\ &\left. + \frac{1 + \Lambda_{21}^{tt}}{1 - \Lambda_{12}^{tt}\Lambda_{21}^{tt}} \cdot \left(\frac{\xi_2 + (c + b + 2k)/2}{\sqrt{\left(\xi_2 + (c + b + 2k)/2\right)^2 - \left((b - k)/2\right)^2}} - 1 \right) \right] d\xi_2 \end{aligned} \tag{29}$$

$$\begin{aligned} &K_{\text{II}}(\text{D}) \\ &= \frac{2\tau_c - \mu p^\infty (1 + \cos 2\alpha) + p^\infty \sin 2\alpha}{2\sqrt{\pi a_2}} \int_{-a_2}^{a_2} \sqrt{\frac{a_2 + \xi_2}{a_2 - \xi_2}} \left[1 \right. \\ &\left. + \frac{1 + \Lambda_{21}^{tt}}{1 - \Lambda_{12}^{tt}\Lambda_{21}^{tt}} \cdot \left(\frac{\xi_2 + (c + b + 2k)/2}{\sqrt{\left(\xi_2 + (c + b + 2k)/2\right)^2 - \left((b - k)/2\right)^2}} - 1 \right) \right] d\xi_2 \end{aligned} \tag{30}$$

3. Interaction Analysis of Two Collinear Cracks of Unequal Length

The interaction between the cracks can be analyzed by calculating the ratio of the SIFs for the inner tips and outer

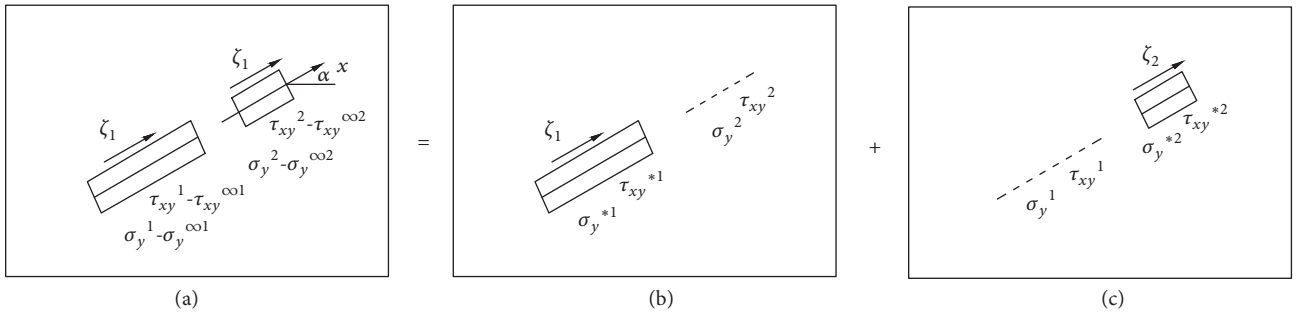

Figure 4: Superposition of stresses for sliding closed collinear cracks.

tips of the cracks (K_I/K_{I0}, K_{II}/K_{II0}), where K_{I0} and K_{II0} are the SIFs when only one crack exists. The influence of the distance between the two cracks can be estimated by keeping the length of the cracks constant and changing the distance. Keeping the length of the large crack and the distance between the two cracks constant, we can analyze the impact of the small crack on the large one by changing the length of the small crack. Similarly, the impact of the large crack on the small one can be analyzed. The research results in [28] show that there is almost no interaction between the two cracks of equal length when the crack distance is equal to twice the half length of the crack, and the propagation of cracks is only related to their parameters. From [29], we can find that the SIF ratio of the inner tips is 1.05 when the two cracks are of equal length and the distance is twice half the length of the crack. Thus, in this paper, almost no interaction is considered when the SIF ratios of the inner tips reach 1.05.

For sliding closed cracks, the crack tips only have K_{II}. The SIF at the crack tips is $K_{II0} = (\tau_{xy}^{\infty} + \tau_c - \mu\sigma_y^{\infty})\sqrt{\pi a}$ when there is only one sliding closed crack in the infinite plate. According to (27) ~ (30), the ratio K_{II}/K_{II0} of the sliding closed cracks is equal to the ratio K_I/K_{I0} of the cracks under uniform tension. Thus, the interaction rule for two collinear sliding closed cracks will be the same as the interaction rule for two collinear cracks subjected to uniform tension.

3.1. The Influence of the Crack Distance. Table 1 shows the results for two collinear cracks of unequal length, while the distance between the inner tips of the two cracks is different and the length of the large crack is different. This table highlights the influence of crack distance and the impact of the large crack length on the small crack. The SIFs of the two cracks, whether at the inner tips or at the outer tips, are larger when another crack exists. K_0 ($K_0 = K_{I0}, K_{II0}$) is the SIF when only one crack exists.

Taking Figure 5 as an example, keeping the length of the two cracks constant, the decrement for the inner tip of the small crack is found to be the largest, and the decrement for the outer tip of the large crack is found to be the smallest. In this paper, it is considered that there is almost no interaction between two cracks if the SIF ratio for the inner tips reaches 1.05. Thus, from Table 1 and Figure 5, we found that there is almost no impact from the small crack on the large crack when the crack distance increases to the length of the small crack, and there is almost no interaction between the two unequal collinear cracks when the crack distance increases to the length of the large crack.

3.2. The Influence of the Large Crack. Keeping the crack distance and the length of the small crack constant in Table 1, it can be obtained that the SIFs for the small crack increase with the increasing length of the large crack, but the SIFs for the large crack decrease. Taking Figure 6 as an example, the trend of the SIFs for the small crack almost increases linearly. The inner tip increases slightly more than the outer tip. The large crack begins to have obvious impact on the inner tip of the small crack when its length increases to the crack distance. When the large crack length increases to one-and-a-half times the crack distance, it will impact the outer tip of the small crack. The influence increases continually with the increasing length of the large crack. However, the increasing large crack length has little influence on itself.

3.3. The Influence of the Small Crack. The impact of the small crack on the large one can be analyzed by keeping the crack distance and the length of the large crack constant. In Figure 7, with the decreasing length of the small crack, the SIF at the inner tip of the large crack is observed to decrease more drastically than the outer tip. However, the SIFs for the small crack are found to increase gradually. This result indicates that the influence of the small crack on the large one is weakening but it is greatly influenced by the large crack as the length of small crack decreases. In Figure 7(a), the SIF ratio for the inner tip of the large crack is less than 1.05 when the small crack length decreases to the crack distance. Thus, it is postulated that the small crack has almost no influence on the large one. In Figure 7(b), under the condition of $d=2a_1$, the SIF ratios for the large crack are all under 1.05 regardless of the length of the small crack. When the small crack length becomes equal to the crack distance (at this time $a_1 = a_2$), there is almost no interaction between the two cracks.

4. Uniaxial Compression Test for Cement Specimen Containing Two Unequal Collinear Cracks

4.1. Specimen Production and Test Equipment. The cement mortar specimen is made of 425 ordinary Portland cement, sand of particle size less than 2 mm, and water. The mixture

Table 1: Results for two collinear cracks of unequal length (a_2=0.4).

d/a_2	$K_I(A)/K_{I0}$				$K_I(B)/K_{I0}$				$K_I(C)/K_{I0}$				$K_I(D)/K_{I0}$			
	a_1=1.5a_2	a_1=2a_2	a_1=3a_2	a_1=4a_2	a_1=1.5a_2	a_1=2a_2	a_1=3a_2	a_1=4a_2	a_1=1.5a_2	a_1=2a_2	a_1=3a_2	a_1=4a_2	a_1=1.5a_2	a_1=2a_2	a_1=3a_2	a_1=4a_2
1	1.0381	1.0301	1.0211	1.0161	1.1043	1.0993	1.0931	1.0894	1.1844	1.2553	1.3896	1.5136	1.0908	1.1319	1.2143	1.2942
2	1.0217	1.0176	1.0128	1.0099	1.0449	1.0427	1.0398	1.0380	1.0856	1.1253	1.2056	1.2839	1.0520	1.0785	1.1344	1.1911
3	1.0144	1.0120	1.0089	1.0071	1.0256	1.0244	1.0228	1.0216	1.0508	1.0769	1.1322	1.1884	1.0343	1.0531	1.0943	1.1374
4	1.0103	1.0088	1.0067	1.0054	1.0167	1.0160	1.0149	1.0142	1.0339	1.0526	1.0935	1.1365	1.0245	1.0387	1.0705	1.1047
5	1.0078	1.0067	1.0053	1.0043	1.0118	1.0113	1.0106	1.0101	1.0244	1.0384	1.0701	1.1043	1.0185	1.0295	1.0549	1.0829
6	1.0061	1.0054	1.0043	1.0035	1.0088	1.0085	1.0079	1.0076	1.0184	1.0294	1.0548	1.0826	1.0144	1.0233	1.0441	1.0674
8	1.0041	1.0036	1.0029	1.0025	1.0055	1.0053	1.0049	1.0047	1.0116	1.0189	1.0362	1.0559	1.0095	1.0156	1.0304	1.0474

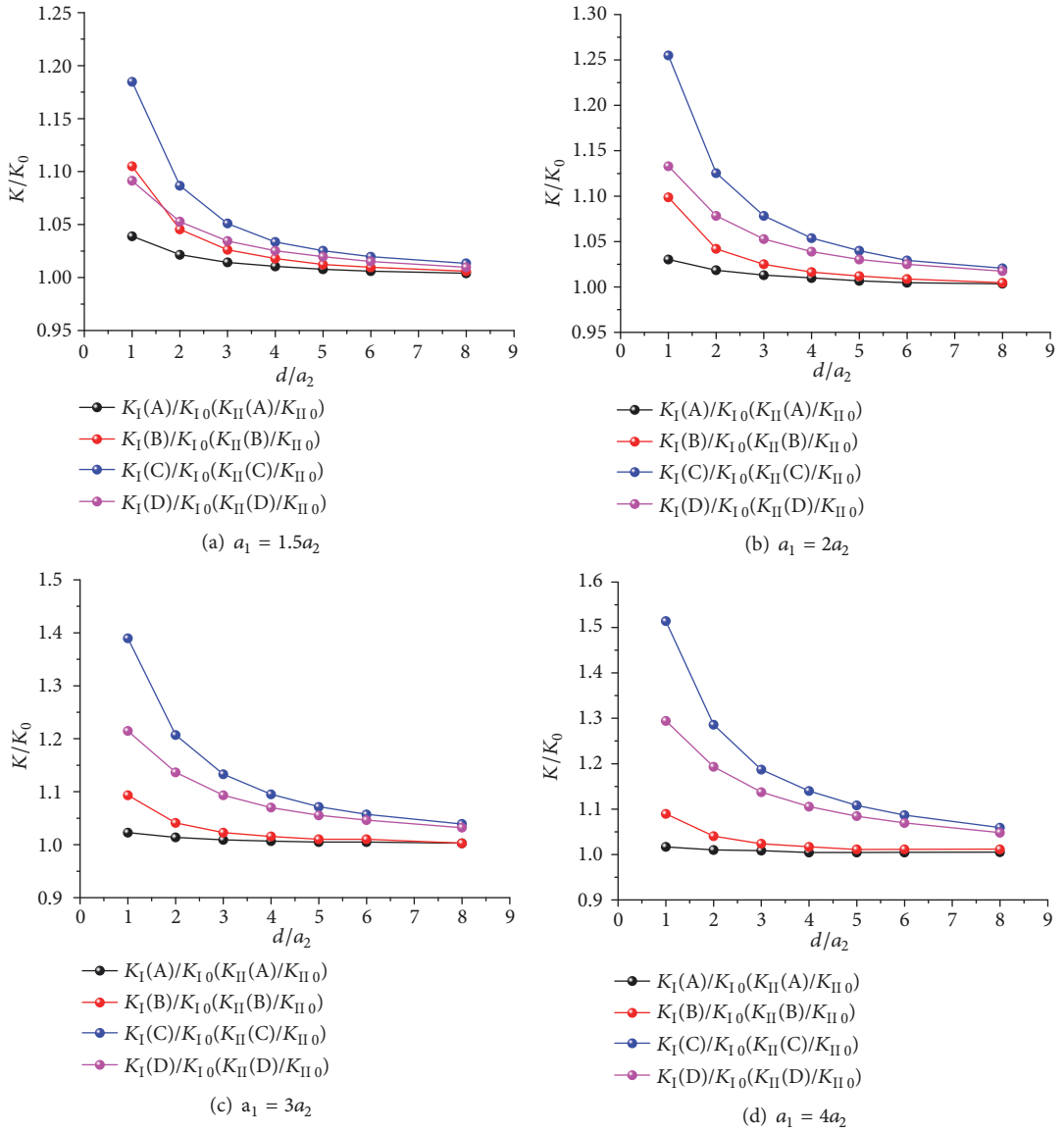

Figure 5: The influence of the crack distance.

ratio (mass ratio) of cement, sand, and water is 1:2.35:0.5. The size of the cement mortar specimen is 110 mm × 110 mm × 30 mm in this test. Two unequal collinear cracks are produced by inserting 0.5 mm thin steel pieces into the cement mortar specimen. The cracks in this test are of three lengths: 24 mm, 18 mm, and 12 mm. Each specimen is cured in a constant temperature and humidity curing room for 12 h, and then the thin steel pieces are pulled out. Next, each specimen is cured for another 12 h before stripping. After stripping, each specimen is cured for 28 days continually. The cement mortar specimen is loaded by the 3000 kN ultrahigh rigidity servo testing machine (Figure 8(a)) in the State Key Laboratory of Coal Resources and Safe Mining of China University of Mining & Technology, Beijing. The loading method is the displacement control loading method, and the loading rate is 0.2 mm/min. A high-speed movie camera (Figure 8(b)) is used to collect the image information during the loading process. The resolution of the high-speed movie camera is 896 × 896, and the shooting speed is set as 50 fps, which ensures that the high-speed movie camera will have enough time to record the entire process of crack initiation, propagation, coalescence, and failure.

The uniaxial compression test considered six specimens, each of which includes two collinear cracks of unequal length. Table 2 lists the geometrical parameters of the two cracks, and the mechanical parameters of the cement mortar specimens are presented in Table 3.

4.2. Propagation of the Cracks. Figure 9 shows the final failure modes of specimen 1, specimen 2, and specimen 3. In Figure 9(a), the inner tips of the two cracks remain close, and shear failure occurred at the bridge area. In Figures 9(b) and 9(c), with the increase of the distance between the inner tips of the two cracks, the failure mode of the bridge

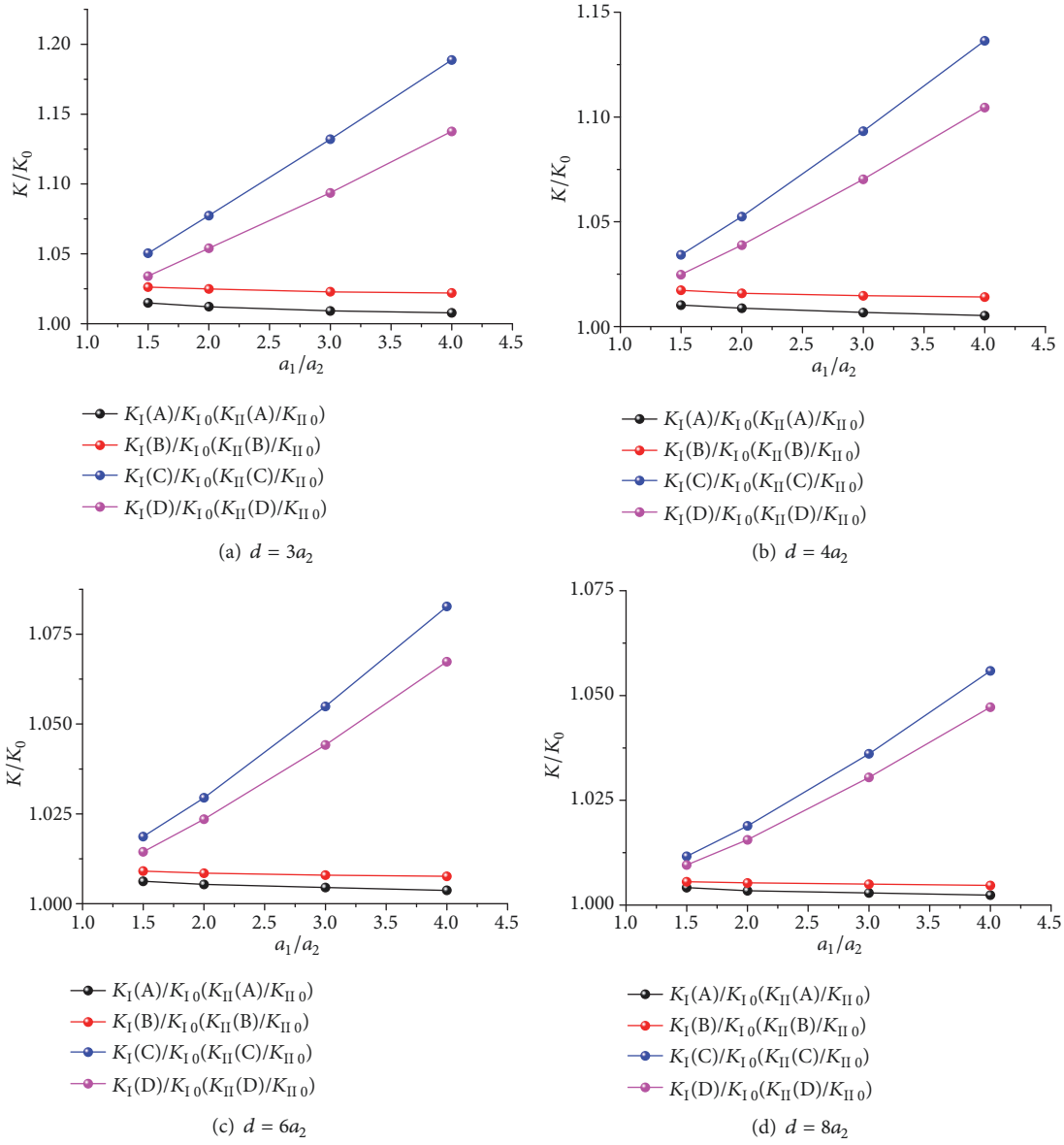

Figure 6: The influence of the large crack.

area changes from the shear failure mode to the tension-shear mixed failure mode. The cracks start to grow from the crack tips. The propagation of the wing crack extends parallel to the maximum compressive stress. Because of the stress concentration, the secondary shear crack may first grow along the direction incline with the crack surface and then tends to reach paths along the crack extension.

In the previous section, the interaction between the two unequal collinear cracks was found to be nearly negligible when the crack distance increases to the length of the large crack. This result is obtained via theoretical analysis. Thus, in this section, the task is to determine whether the test result is in agreement with the theoretical result. Figures 9(d) and 9(e) show that only the two tips of the large crack initiate the wing crack and that this wing crack extends parallel to the maximum compressive stress. The small crack remains intact. In Figure 9(f), the small crack initiated microcracks, but the growth of the microcracks is not clear. The large crack and the small crack in the three specimens, respectively, grow under compression and do not affect each other. This result indicates that the interaction between the two cracks is very weak when the crack distance between the two collinear cracks reaches the length of the large cracks. This test result is in agreement with the theoretical result obtained in the previous section.

When the inclination angle of the collinear cracks is 45°, the stress-strain curves of the specimen 1 to specimen 4 tested by the uniaxial compression experiment are obtained in Figure 10. From the curves (a) ~ (d), it can be seen that the cracks in specimen 1 ~ 4 initiate when the axial stress is 26MPa, 27.9MPa, 33.1MPa, and 34.4MPa, respectively, and the wing cracks always appear at the inner tip of the large crack in the uniaxial compression test. The stress

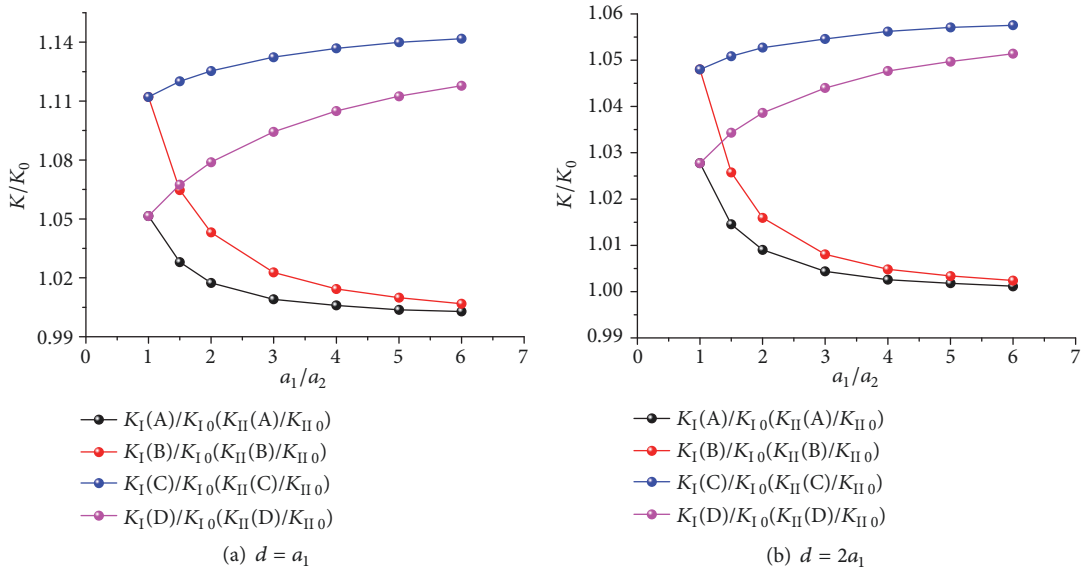

Figure 7: The influence of the small crack.

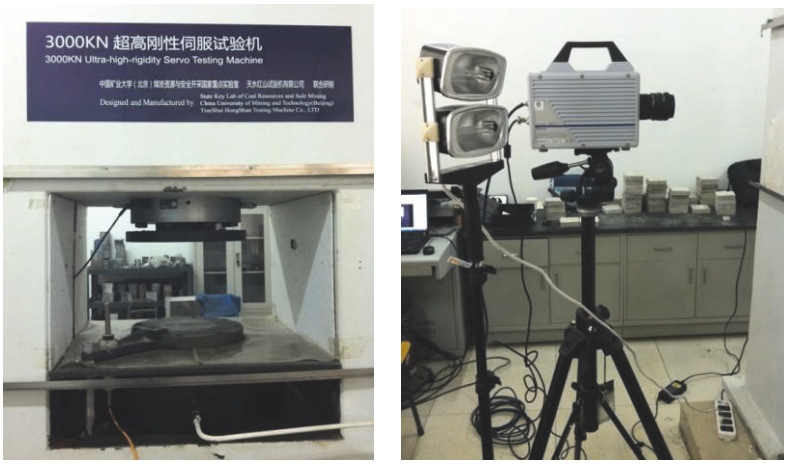

(a) 3000 kN ultrahigh rigidity servo testing machine

(b) FASRCAM SA1.1 high-speed movie camera

Figure 8: The pieces of test equipment.

Table 2: Geometric parameters of two collinear cracks of unequal length in the cement mortar specimens.

Specimen number	Incline angle α	The large crack length $2a_1$	The distance d	The small crack length $2a_2$
1	45°	24 mm	6 mm	12 mm
2	45°	24 mm	12 mm	12 mm
3	45°	24 mm	18 mm	12 mm
4	45°	24 mm	24 mm	12 mm
5	60°	24 mm	24 mm	12 mm
6	30°	24 mm	24 mm	12 mm

Table 3: Mechanical parameters of the specimen.

Density /kg/m^3	elastic modulus /GPa	Uniaxial compressive strength /MPa	Uniaxial tensile strength /MPa	Poisson ratio	K_{Ic}/(MPa·m$^{1/2}$)
2350	15.2	55	2.3	0.15	0.59

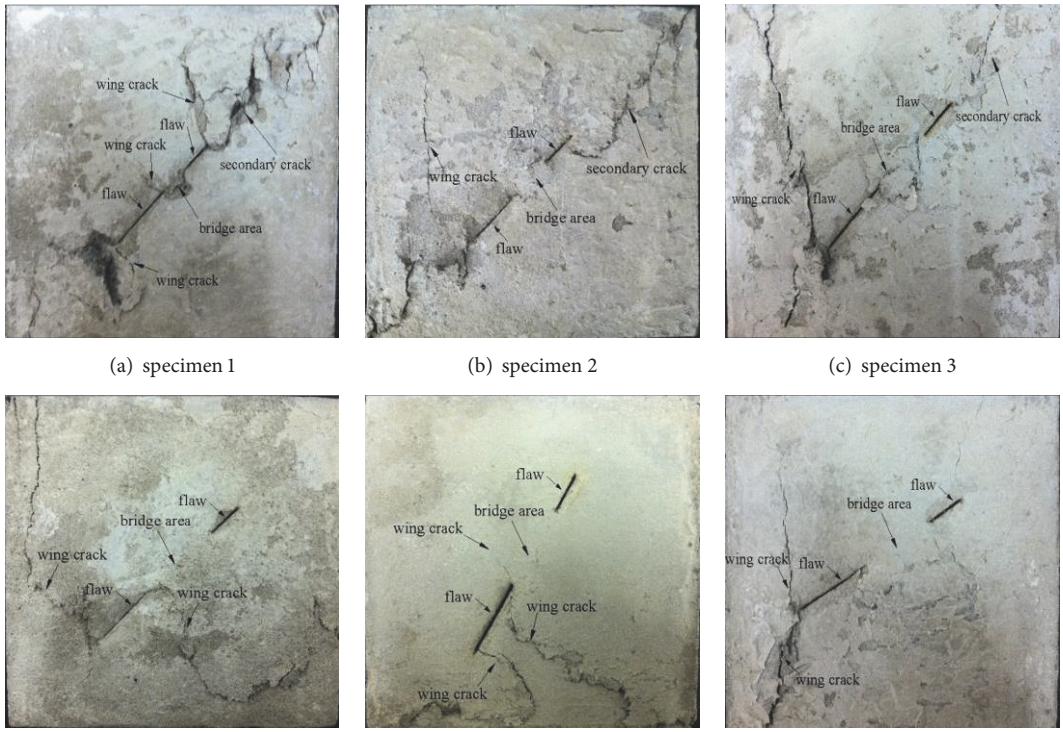

(a) specimen 1 (b) specimen 2 (c) specimen 3

(d) specimen 4 (e) specimen 5 (f) specimen 6

Figure 9: Propagation of the two unequal collinear cracks loaded by uniaxial compression.

value at this time is usually referred to as the crack initial stress. When the axial stress of specimen 1 ~ 3 increases to 41.2MPa, 45.3MPa, and 46.7MPa, respectively, the crack further propagates and the rock bridge between cracks is penetrated, but the rock bridge between cracks in specimen 4 is not perforated, which is mainly due to the excessive spacing between cracks. The phenomenon is consistent with the theoretical analysis conclusions above. According to the stress-strain curves shown in Figure 10, the variation of crack initial stress and peak stress of the specimens 1-4 is shown as shown in Figure 11. As can be seen from Figure 11, the peak stress of the specimens containing cracks is lower than that in an intact specimen, which indicates that the existence of cracks has obvious influence on the strength of the specimens. The peak stress and the initial stress both increase with the increasing of the crack distance, which mainly occurs because of the relationship that the longer the crack distance, the weaker the crack interaction. Thus, the influence of crack propagation on the strength of the specimen is weaker.

5. Numerical Analysis of Interaction and Propagation of Unequal Length Collinear Cracks

Rock fracture process analysis system RFPA^{2D} is a numerical test tool based on finite element theory and statistical damage theory, which fully considers the characteristics of rock fracture inhomogeneity and anisotropy, and can simulate the progressive failure of materials. Its reliability has been verified [30]. RFPA^{2D} can well consider the inhomogeneity of rock medium through the model parameter m. The larger m is, the more uniform the rock is, and the smaller m is, and the more uneven the rock is. In this simulation, m ≥ 5 is taken, and the other model parameters are selected according to the parameters measured by similar material tests. As shown in Table 4, the physical and mechanical properties of the model are close to those of sandstone. Because rock is a kind of brittle heavy material, its tensile strength is much lower than its compressive strength, so the modified Mohr-Coulomb criterion is used as the strength criterion of model element failure in this simulation.

Three groups of unequal length collinear double crack specimens with inclination angles of 45° were presetted. The double crack lengths are 24 mm and 12 mm, respectively, in which the crack spacing of the first group of specimens (a) is 6 mm, the crack spacing of the second group of specimen (b) is 12 mm, and the spacing of the third group of specimens (c) is 24mm. The specimen size of 110 mm×110 mm is divided into 330 × 330 equal area units and plane strain analysis was used in the simulation. The numerical tests of three groups of specimens under uniaxial tension and uniaxial compression were carried out by using vertical stress loading in the simulation process. Each step of the uniaxial tension process is loaded with 0.02 MPa, and each step of the uniaxial compression process is loaded with 0.2MPa.

Figure 12 shows the maximum shear stress diagrams for the propagation of three groups of unequal length collinear

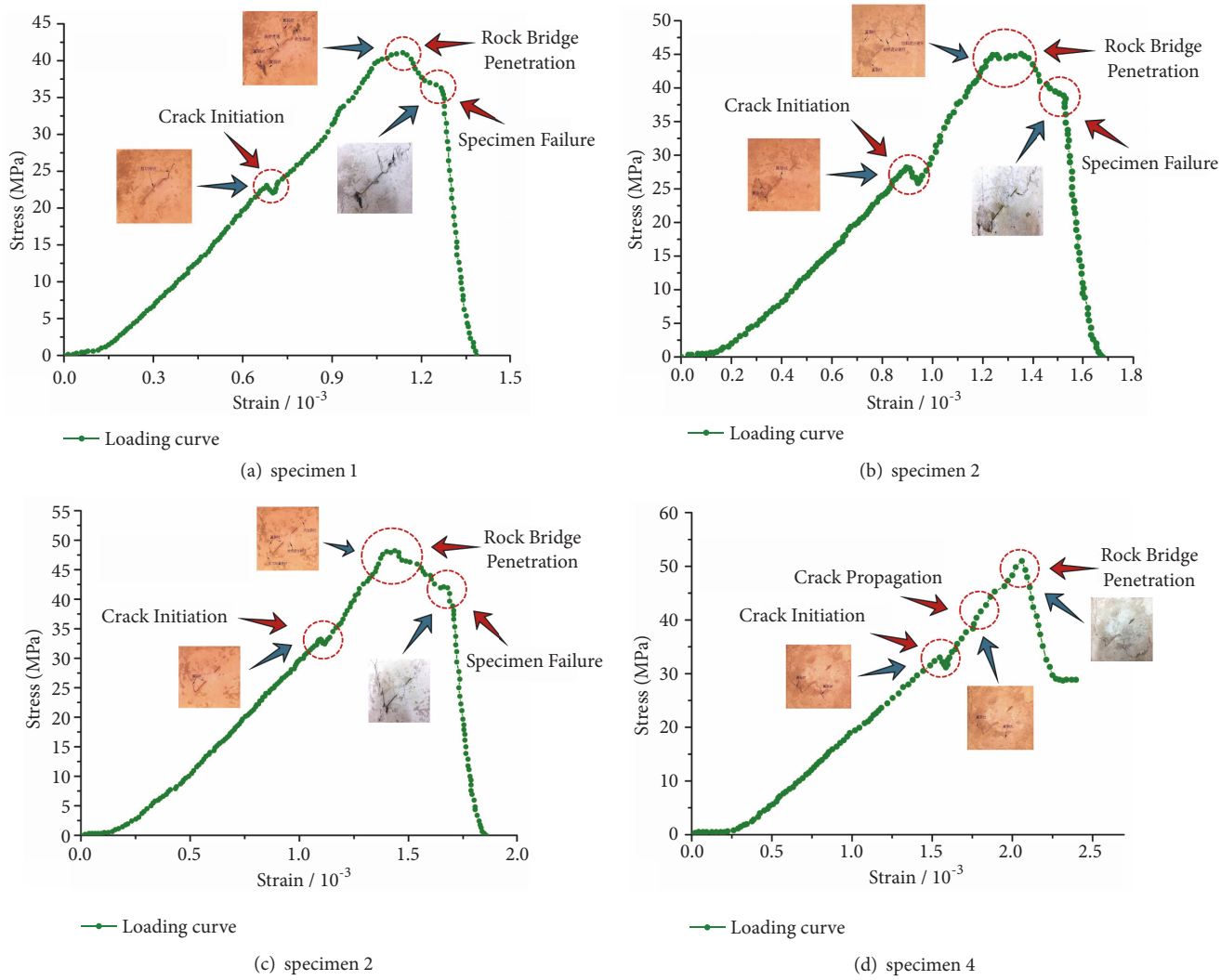

Figure 10: Stress-strain curves of each specimen during uniaxial loading.

Table 4: Parameters of numerical model.

Materials	Elastic modulus / GPa	Density / kg·m^{-3}	Internal friction angle /°	Poisson ratio	Average compressive strength / MPa
Sandstone	10 ~ 100	2000 ~ 2600	4 ~ 25	0.1 ~ 0.3	20 ~ 200
Model	15.2	2350	30	0.15	53

bicracks under uniaxial tension (the brightness of the element in the figure indicates the magnitude of the stress, and the brighter the element, the greater the stress of the element). It can be seen from Figure 12 that the stress at the tip of the large crack is the largest in all three groups of specimens, and the inner tip of the large crack is the easiest to initiate under uniaxial action. The crack spacing of the first group of specimens is small, which is equal to the half-length of the small crack. Under the action of axial stress, the inner and outer tip of the large crack first germinate the wing crack with the increasing of the stress, and the small crack forms a secondary crack at the inner tip of it, and the secondary crack overlaps with the end wing crack to cause the rock bridge to penetrate. The bearing capacity of the specimen decreases rapidly, which eventually leads to the overall failure of the specimen. The wing crack occurs at the inner tip of the large crack in the second group of specimens, followed by the wing crack at the outer end of the large crack. With the continuous propagation of the wing crack, the specimen is finally destroyed and the rock bridge is not penetrating. The crack spacing of the third group is large, which is equal to the length of the large crack. When loading a certain

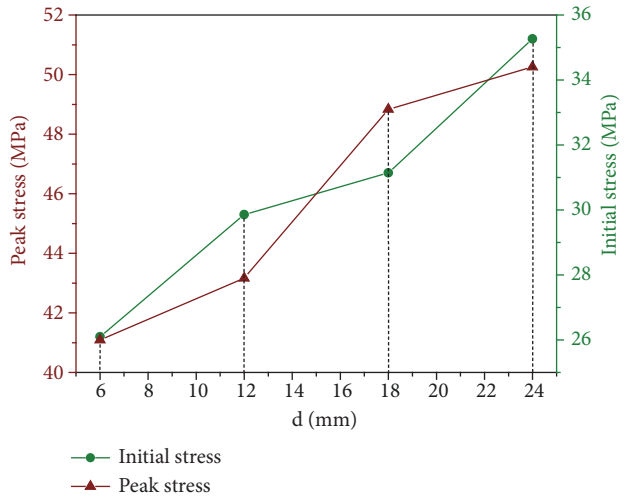

Figure 11: Relationship of the peak stress and the initial stress and the crack distance.

stress, the wing crack occurs at both ends of the large crack and propagates continuously, which leads to the failure of the specimen, but the rock bridge is impenetrable and the small crack is almost intact. The crack propagation direction of the three groups of specimens is finally approximately perpendicular to the stress loading direction, and with the increasing of crack spacing, the propagation of small cracks becomes weaker and weaker, which indicates that the effect of large cracks on small cracks is decreasing. When the crack spacing increases to equal to the length of the large crack, there is almost no interaction between the two cracks, which is consistent with the above theoretical results.

Figure 13 shows the maximum shear stress diagram of cracks under uniaxial compression of three groups of specimens. When the crack is subjected to uniaxial compression, the tip of the two sides of the large crack will first initiate the wing crack. If the crack spacing is small, the small crack at the tip of the large crack will overlap with the wing crack at the tip of the small crack, resulting in the penetration of the rock bridge and finally the failure of the specimen. If the crack spacing is large, the failure of the specimen is mainly caused by the continuous propagation of the wing crack. When the crack spacing is larger than the length of the large crack, the propagation of the two cracks does not affect each other under the action of stress, and the crack propagates along the loading direction parallel to the force. The conclusions are in good agreement with the theoretical and experimental results above.

6. Conclusion

Based on the Kachanov method, the expressions for the stress intensity factor of two unequal collinear cracks were derived to analyze the interaction between the two cracks. The influence of the crack length and crack distance on the crack interaction was analyzed, and a compression test of the cement mortar specimen containing two unequal collinear cracks was performed. The conclusions of this study are as follows.

(1) For collinear cracks, whether subjected to uniaxial tension or compression, the influence degree of the crack length and the crack distance on the crack interaction is the same. There is almost no interaction between the two unequal collinear cracks when the crack distance increases to the length of the large crack.

(2) The impact of the large crack on the small one becomes obvious when the length of the large crack increases to the crack distance. The impact of the small crack length on the large one almost disappears when the length of the small crack decreases to the distance between the two cracks.

(3) Shear failure occurs in the bridge area when the crack distance is very close, and the failure mode changes to mixed-mode failure with the increase of the crack distance. When the crack distance reaches the large crack length, the two respective cracks grow under compression and do not affect each other. This test result is in agreement with the theoretical result.

Appendix

A.

Consider two cracks 'i' and 'j', as shown in Figure 14; the interaction coefficients in (3) and (4) can be obtained as [3]

$$f_{ij}^{nn} - if_{ij}^{nt} = \int_{-a_i}^{a_i} \left(\overline{f}_{ij}^{nn} - i\overline{f}_{ij}^{nt}\right) d\xi_i \tag{A.1}$$

$$f_{ij}^{tn} - if_{ij}^{tt} = \int_{-a_i}^{a_i} \left(\overline{f}_{ij}^{tn} - i\overline{f}_{ij}^{tt}\right) d\xi_i \tag{A.2}$$

$$\Lambda_{ij}^{kl} = \frac{1}{2a_j} \int_{-a_j}^{a_j} f_{ij}^{kl} d\xi_j 1 \quad (k,l = n,t) \tag{A.3}$$

where

$$\overline{f_{ij}^{nn}} - i\overline{f_{ij}^{nt}} = \frac{\sqrt{a_i^2 - \xi_i^2}}{2\pi} \left[G(z) + \overline{G(z)} + e^{-2i\alpha_j}(z - \overline{z})\overline{G'(z)}\right] \tag{A.4}$$

$$\overline{f_{ij}^{tn}} - i\overline{f_{ij}^{tt}} = -\frac{\sqrt{a_i^2 - \xi_i^2}}{2\pi i} \left[\overline{G(z)}\left(1 - 2e^{-2i\alpha_i}\right) - G(z) + e^{-2i\alpha_j}(z - \overline{z})\overline{G'(z)}\right] \tag{A.5}$$

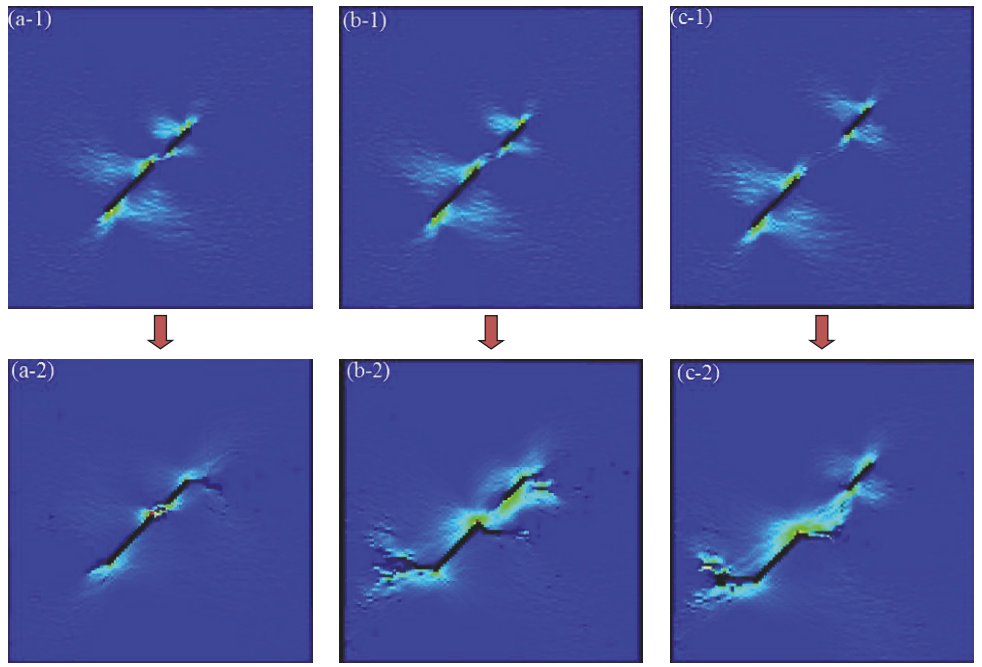

Figure 12: Propagation and fracture of the unequal collinear cracks under uniaxial tension in the three samples.

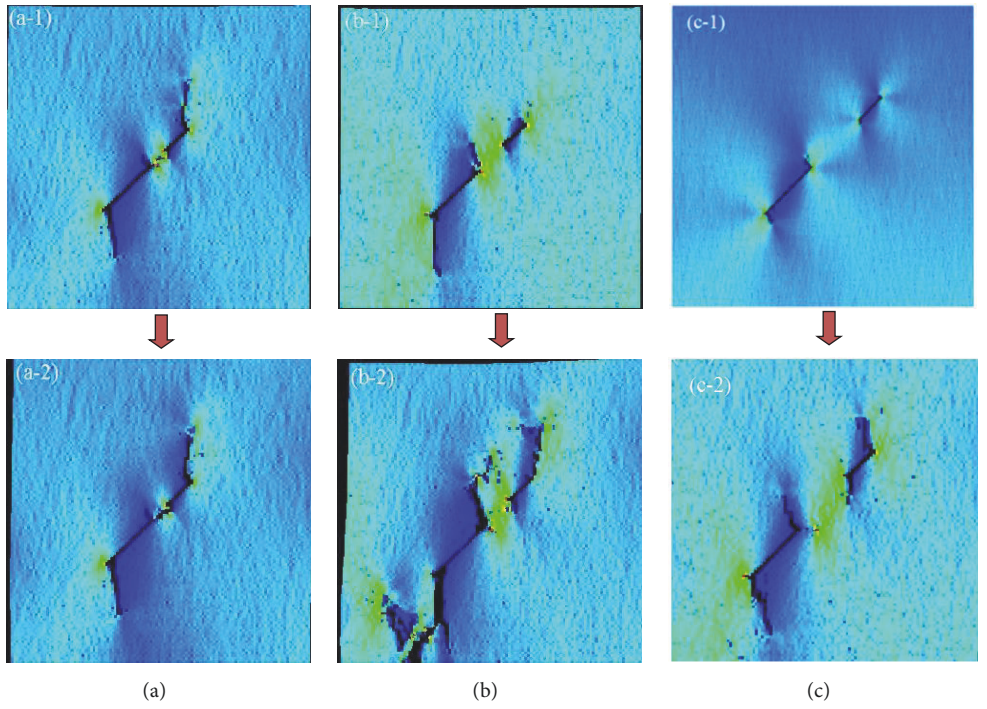

Figure 13: Propagation and fracture of the unequal collinear cracks under uniaxial compression in the three samples.

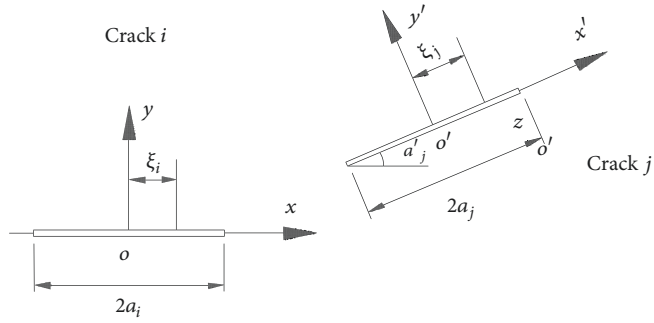

Figure 14: Cracks 'i' and 'j'.

where $z = z(\xi_j)$ is the complex coordinate in x-o-y coordinate system of the point $(\xi_j,0)$ in crack 'j' and

$$G(z) = \frac{1}{(z-\xi_i)\sqrt{z^2-a_i^2}} \tag{A.6}$$

$$G'(z) = \frac{a_i^2 + \xi_i z - 2z^2}{(z-\xi_i)^2\left(\sqrt{z^2-a_i^2}\right)^3} \tag{A.7}$$

In the above equations, 'i' denotes the imaginary unit.

B.

Once the tractions $p(\xi) = [\sigma_n \ \ \sigma_t]^T$ on cracks are determined, the SIFs at crack tips are [1] as follows:

$$\begin{Bmatrix} K_{\mathrm{I}}(\pm a) \\ K_{\Pi}(\pm a) \end{Bmatrix} = \frac{1}{\sqrt{\pi a}} \int_{-a}^{a} \sqrt{\frac{a \pm \xi}{a \mp \xi}} \begin{Bmatrix} -\sigma_n(\xi) \\ -\sigma_t(\xi) \end{Bmatrix} d\xi \tag{B.1}$$

Data Availability

The data used to support the findings of this study are currently under embargo while the research findings are commercialized. Requests for data, 6 months after publication of this article, will be considered by the corresponding author.

Conflicts of Interest

The authors declare that they have no conflicts of interest.

Acknowledgments

The authors acknowledge financial support from the Project Supported by the Special Fund of Shanxi Scholars Support Plan (No. 2050205).

References

[1] I. N. Sneddon and M. Lowengrub, *Crack Problems in the Classical Theory of Elasticity*, Wiley, New York, NY, USA, 1969.

[2] F. Erdogan, "Stress intensity factors," *Journal of Applied Mechanics*, vol. 50, pp. 992–1002, 1983.

[3] Y. Z. Chen, "Multiple crack problems of antiplane elasticity in an infinite body," *Engineering Fracture Mechanics*, vol. 20, no. 5-6, pp. 767–775, 1984.

[4] Y. Z. Chen, "Numerical solution for multiple crack problem in an infinite plate under compression," *International Journal of Fracture*, vol. 129, no. 1, pp. 51–62, 2004.

[5] K. Y. Lam and S. P. Phua, "Multiple crack interaction and its effect on stress intensity factor," *Engineering Fracture Mechanics*, vol. 40, no. 3, pp. 585–591, 1991.

[6] Z. Y. Ren, W. D. Pan, S. M. Liu et al., "Numerical simulation of non-parallel double crack propagation and coalescence in rock specimen," *Journal of Mining Science and Technology*, vol. 2, no. 1, pp. 33–41, 2017.

[7] Y. Z. Chen, "Solutions of multiple crack problems of a circular plate or an infinite plate containing a circular hole by using Fredholm integral equation approach," *International Journal of Fracture*, vol. 25, no. 3, pp. 155–168, 1984.

[8] X. Huang and B. L. Karihaloo, "Tension softening of quasi-brittle materials modelled by singly and doubly periodic arrays of coplanar penny-shaped cracks," *Mechanics of Materials*, vol. 13, no. 3, pp. 257–275, 1992.

[9] X. Huang and B. L. Karihaloo, "Interaction of penny-shaped cracks with a half-plane crack," *International Journal of Solids and Structures*, vol. 30, no. 15, pp. 2117–2139, 1993.

[10] B. L. Karihaloo and X. Huang, "Asymptotics of three-dimensional macrocrack-microcrack interaction," *International Journal of Solids and Structures*, vol. 32, no. 11, pp. 1495–1500, 1995.

[11] H. Horii and S. Nemat-Nasser, "Compression-induced microcrack growth in brittle solids: Axial splitting and shear failure," *Journal of Geophysical Research: Atmospheres*, vol. 90, no. B4, pp. 3105–3125, 1985.

[12] H. Horii and S. Nemat-Nasser, "Elastic fields of interacting inhomogeneities," *International Journal of Solids and Structures*, vol. 21, no. 7, pp. 731–745, 1985.

[13] S. X. Gong, "Microcrack interaction with a finite main crack: an exact formulation," *International Journal of Fracture*, vol. 66, no. 3, pp. R51–R56, 1994.

[14] M. Kachanov, "Elastic solids with many cracks: a simple method of analysis," *International Journal of Solids and Structures*, vol. 23, no. 1, pp. 23–43, 1987.

[15] M. Kachanov, "A simple technique of stress analysis in elastic solids with many cracks," *International Journal of Fracture*, vol. 28, pp. 11–19, 1985.

[16] L. Gorbatikh and M. Kachanov, "A simple technique for constructing the full stress and displacement fields in elastic plates with multiple cracks," *Engineering Fracture Mechanics*, vol. 66, no. 1, pp. 51–63, 2000.

[17] M. Kachanov, "Effective elastic properties of cracked solids: critical review of some basic concepts," *Applied Mechanics Reviews*, vol. 45, no. 8, pp. 304–335, 1992.

[18] A. Chudnovsky and M. Kachanov, "Interaction of a crack with a field of microcracks," *International Journal of Engineering Science*, vol. 21, no. 8, pp. 1009–1018, 1983.

[19] J. H. Kuang and C. K. Chen, "Alternating iteration method for interacting multiple crack problems," *Fatigue Fracture of Engineering Materials and Structures*, vol. 22, no. 9, pp. 743–752, 1999.

[20] M. Basista and D. Gross, "A note on crack interactions under compression," *International Journal of Fracture*, vol. 102, pp. L67–L72, 2000.

[21] D. Gross, "Stress intensity factors of systems of cracks," *Ingenieur-Archiv*, vol. 51, no. 5, pp. 301–310, 1982.

[22] J. Wang, J. Fang, and B. L. Karihaloo, "Asymptotics of multiple crack interactions and prediction of effective modulus," *International Journal of Solids and Structures*, vol. 37, no. 31, pp. 4261–4273, 2000.

[23] Y. P. Li, L. G. Tham, Y. H. Wang, and Y. Tsui, "A modified Kachanov method for analysis of solids with multiple cracks," *Engineering Fracture Mechanics*, vol. 70, no. 9, pp. 1115–1129, 2003.

[24] H. Qing and W. Yang, "Characterization of strongly interacted multiple cracks in an infinite plate," *Theoretical and Applied Fracture Mechanics*, vol. 46, no. 3, pp. 209–216, 2006.

[25] M. F. Ashby and S. D. Hallam, "The failure of brittle solids containing small cracks under compressive stress states," *Acta Metallurgica et Materialia*, vol. 34, no. 3, pp. 497–510, 1986.

[26] A. Bobet and H. H. Einstein, "Fracture coalescence in rock-type materials under uniaxial and biaxial compression," *International Journal of Rock Mechanics and Mining Sciences*, vol. 35, no. 7, pp. 863–888, 1998.

[27] O. Reyes and H. H. Einstein, "Failure Mechanisms of Fractured Rock - A Fracture Coalescence Model," in *Proceedings of the 7th International Conference on Rock Mechanics*, pp. 333–340, 1991.

[28] P. Zhang, R. L. He, N. Li, and X. B. Li, "Uniaxial compressive strength analysis of fractured media containing intermittent fractures at different strain rates," *Chinese Journal of Rock Mechanics and Engineering*, vol. 26, pp. 2735–2742, 2007.

[29] Chinese Aeronautical Establishment, *Handbook of Stress Intensity Factors*, Science Press, Beijing, China, 1981.

[30] C. A. Tang and S. Q. Kou, "Crack propagation and coalescence in brittle materials under compression," *Engineering Fracture Mechanics*, vol. 61, no. 3-4, pp. 311–324, 1998.